Available online at www.sciencedirect.com
ScienceDirect
Journal of Sound and Vibration 323 (2009) 313–333
JOURNAL OF SOUND AND VIBRATION
www.elsevier.com/locate/jsvi

Measurement of the kinematics of two underplatform dampers with different geometry and comparison with numerical simulation

Christian M. Firrone*

Department of Mechanical Engineering, Politecnico di Torino, Corso Duca degli Abruzzi, 24 10129-Turin, Italy

Received 22 April 2008; received in revised form 3 December 2008; accepted 3 December 2008
Handling Editor: C.L. Morfey
Available online 31 January 2009

Abstract

Underplatform dampers are used as friction damping devices in order to reduce the amplitude of vibrations of blades in turbine rotors. In this paper a study was performed on the forced response of a mock up system which simulates the flexural behaviour of two turbine blades with an interposed underplatform damper. Two different geometries are tested for two different deflection shapes and the dynamic response of the whole system is explained with respect to the damper kinematics. The originality of the work consists in the measurement of the damper displacements by means of a laser Doppler vibrometers (LDV) equipment and in the comparison with the displacements obtained by numerical predictions of a numerical code used for damper design. The strong influence of the rotation of the underplatform damper on the dynamic response is analysed in particular for the in-phase vibration of the two dummy blades. Comparison between calculations and experiments shows that the damper model allows simulating the damper kinematics with good accuracy.
© 2008 Elsevier Ltd. All rights reserved.

1. Introduction

Widespread up to date technological devices aimed at reducing the blade vibration of rotating turbo machinery are based on the use of friction damping. Slip phenomena coming from: (i) blade root joint, (ii) blade interlocking at blade tip or along its height through shrouds, and (iii) slipping motion of underplatform dampers located between two neighbouring blades, are studied to limit the amplitude of oscillation and the consequent HCF damage. Underplatform dampers are metal parts with a given geometry free to move inside a cavity placed underneath the blade airfoils. The centrifugal force due to engine rotation presses the underplatform damper against the blade platforms. When the relative displacements due to gas flow and vibrations coming from engine rotation are large enough to cause slipping at the contact interface, the resulting hysteresis loop dissipates the excitation energy through friction. These passive damping systems are object of preliminary detailed study in order to apply the best combination of geometry and mass to achieve the optimal amplitude reduction during service life.

*Tel.: +39 011 5646953; fax: +39 011 5646999.
E-mail addresses: christian.firrone@polito.it, firrone@hotmail.com (C.M. Firrone).

0022-460X/$ - see front matter © 2008 Elsevier Ltd. All rights reserved.
doi:10.1016/j.jsv.2008.12.019

Ideally the contact surfaces must have an inclination that permits tangential relative displacements large enough to cause slipping. Besides, the contact surface causes a different localized contact region if it is rounded or flat, leading to different pressure distribution inducing macro-slip or micro-slip behaviour. The mass generates the inertial effect of the damper and the centrifugal force which determines the preload on the contact surfaces.

The dynamic behaviour of the blade-underplatform damper system is computed by solving a set of nonlinear balance equations. For this reason many authors have developed numerical codes based on algorithms which iteratively search for the convergence of the solution [1–3]. Results are then validated by test rig experimental measurements. In these test rigs, real or dummy blades are clamped in a fixture and are in contact with one [2,4–6] or two [1] underplatform dampers. They are pressed against blade platforms using wires pulled with an "equivalent centrifugal" force. When two blades are coupled through an underplatform damper, a meaningful range of frequency used to collect nonlinear FRF data includes two modal shapes, the so called: "in phase" (IP) modal shape and 180° "out of phase" (OoP) modal shape. In Fig. 1 the deflections for the two blades are sketched for the two configurations.

It is evident that the stiffness of the test rig differs significantly from the dynamic stiffness of the disc; therefore resonant IP and OoP frequencies of blades in the two conditions will be significantly different. However, relative displacement shapes between blades are substantially the same on disc and on rig, therefore tests on the rig are valid to assess damper performance.

A further remark is that IP motion is normally more critical than OoP. In fact experience shows that dampers are generally less effective in IP modes, while IP excitation may be dominant, particularly for high pressure turbine stages near to the combustion chambers.

A lot of literature has been produced about this topic [7]. Given for example a low engine order EO = 6 for a turbine with 100 blades, it is simple to calculate how the phase delay of the excitation harmonic force of two contiguous blades is about 0.38 rad. If this force pattern should excite a mode shape of the bladed disk with the nodal diameter equal to the EO at its resonance, the response of the system would benefit from a low amount of damping produced by the underplatform damper, since in this case the relative displacements between contiguous blades are closely similar to an IP deflection shape.

As a consequence, this paper aims at investigating the damping effectiveness of underplatform dampers on a test rig, and gives the same importance to the study of the IP and OoP mode. Two damper shapes are investigated: (i) cylindrical and (ii) 45° symmetric wedge or cottage-roof damper.

Results show that even flat surface couplings, as in cottage roof dampers in IP mode, do not follow the simple slider kinematics and cause a contact rocking motion. The numerical model now in use, and employed throughout this paper to compare calculations with experimental results, includes this rocking motion characteristic at the contact. It will be shown that without this added feature, conventional "slider" contact nodes produce results which are in conflict with experimental observations.

2. Synthesis of the forced response calculation procedure

There are many publications dealing with the underplatform damper design [1–3]. Most of them are especially focused on the development of a computational method for damper mass optimization. Two ingredients are essential to the aim: the contact model and the damper kinematic model.

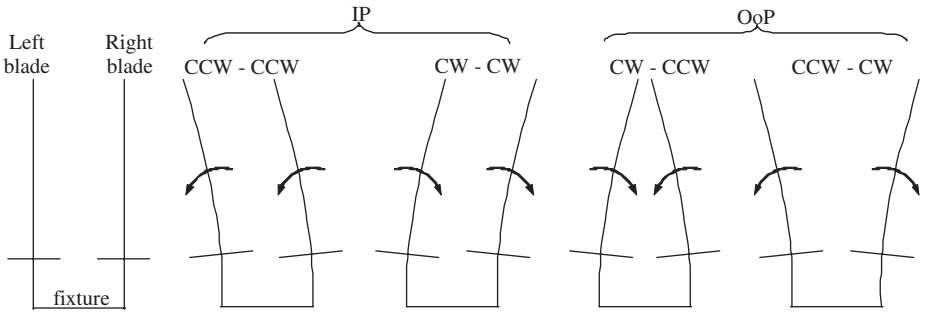

Fig. 1. In phase and out of phase modes (CW: clockwise motion, CCW: counter clockwise motion).

Macro-slip contact model is modelled by single slider application which in past literature was characterized by more and more complete set of constitutive equations: 1D no motion-slip state [8], 1D elastic stick–slip state [9], 2D in plane stick–slip state [10,11], 2D stick–slip-lift off state [12], 3D stick–slip-lift off state [13]. The last two and more complete of these contact models need nonlinear tangential and normal stiffness and friction coefficient to be known. Literature was produced aimed at predicting these values theoretically and experimentally [14–16]. Micro-slip behaviour is in general modelled by means of macro-slip array [5,11], while the analytical approach is used in refined laboratory approaches [17].

The kinematic model consists in the computation of the relative displacements at the contact interface along the tangential and normal direction, in order to calculate the hysteresis loop through contact state transition criteria. The relative motion at the contact surfaces depends on the hypothesis assumed to take into account the presence of the damper, i.e., the damper model.

Earlier publications [6,18] consider the damper model under the following assumption: (i) the damper kinematics is the result of pure translational relative motion between platforms and (ii) the damper is always kept in full surface contact with blade platforms by centrifugal force. Relative displacements at contacts are therefore supposed to be in the contact plane only. The damper has no inertial property, its mass is used only to determine the centrifugal force. Further developments [19,20] include damper inertia; normal and tangential stiffness are modelled by springs connecting a point on each platform surface to the damper centre of mass. In Ref. [2] the real contact regions are taken into account, providing the damper a geometric extension which permits to differentiate the absolute displacements of the left from the right side. The inertial properties are still concentrated in the centre of mass. In Refs. [21,22], mass and elastic properties of the damper are fully taken into account through a finite element model.

The code developed in collaboration with AVIO Group has been described in Ref. [22] and is here used. Its main features are summarized as follows:

- The bladed disk and the underplatform damper are two substructures modelled with FEM, reduced by component mode synthesis including the contact nodes in the set of master nodes (Fig. 2). In the case under analysis the code was used to couple the two dummy blades system of the test rig to one cylindrical and wedge underplatform damper.

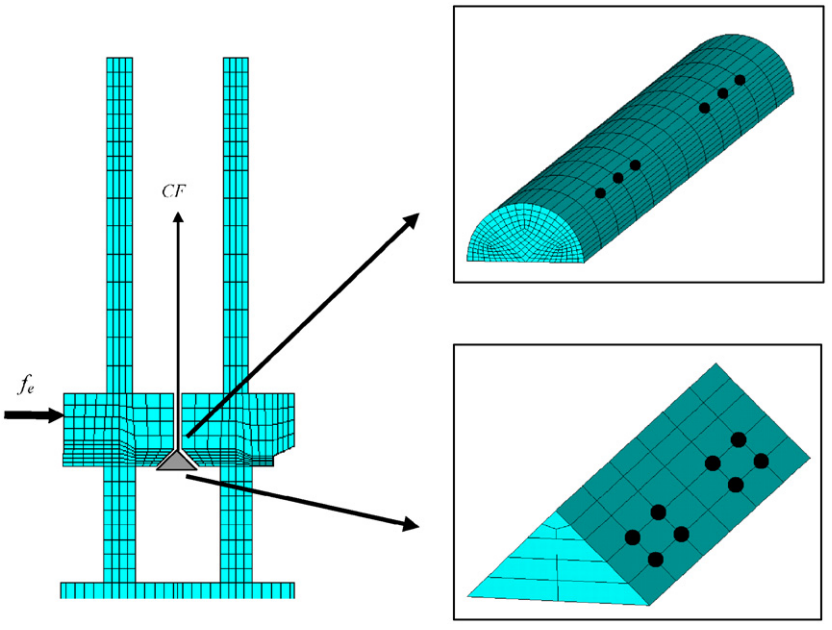

Fig. 2. FE models of the dummy blades and underplatform dampers. Dots on the underplatform dampers indicate the position of the contact elements.

- The two substructures (blades + damper) are coupled in MATLAB using 2D macro-slip contact elements which take into account stick–slip-lift-off state according to [12]. A nonlinear static FE analysis provides the determination of the real contact area, therefore it determines the appropriate position of the contact elements. The simulation is performed by applying the pulling loads exactly in the same position and with the same numerical value used during the tests.
- Harmonic balance method is implemented.
- The iterative solver is based on the Newton–Raphson algorithm.

3. Experimental set-up

Two dummy blades have their base clamped in a hydraulic press by means of a hydraulic cylinder. The cylindrical and wedge underplatform dampers, shown in Figs. 3b and c, are placed in a cavity underneath the blade platforms as shown in Fig. 3a. The inclination of the blade platforms is 45° on either side. The steel wires, passing through the damper, carry a mass M which produces the equivalent of a real operative centrifugal load, $CF = 350$ N. One of the blades is excited by means of an electromagnetic shaker. Stepped sine frequency response testing is performed using controlled constant input-force level, which is measured with a force transducer and kept constant through software control. At each frequency the feedback system adjusts the shaker force in order to obtain an excitation amplitude equal to the nominal value within a tolerance of 5%. If the control loop is not achieved within a transitory time because the system is incapable to deliver the input force level demanded (force drop-off phenomenon), the procedure is repeated for a limited number of times until a maximum iteration number chosen by the user is reached. In this case the system collects the response obtained from the last iteration, then starts to excite the structure with the next frequency value. The response levels of the two blades are measured with four accelerometers placed two at the tip of each blade and two at the blade platforms height (Fig. 3a).

Experimental tests were subjected to repetition in order to obtain reliable data. This includes also the extraction of dampers from the cavity, the cleaning of the contact surfaces and positioning, and the repetition of the tests at a distance of time.

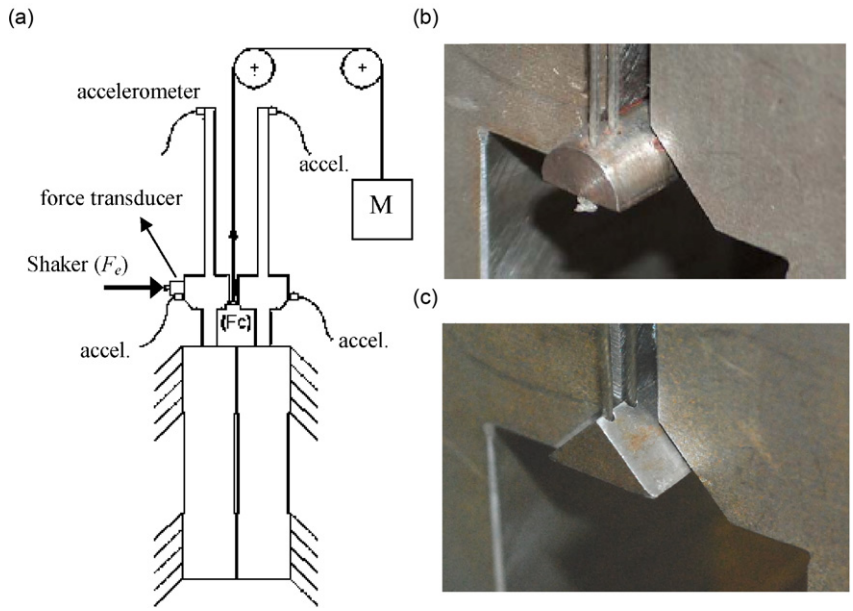

Fig. 3. (a) Sketch of the test rig, (b) cylindrical damper, and (c) wedge damper.

3.1. LDV equipment set-up

Two LDV vibrometers (Polytech OFV-505, calibration error 0.25%, sensitivity 125 mm s^{-1} V^{-1}, Fig. 4a) produce two beams pointed on the base of the dummy blades (Fig. 4b). A 45° prism reflects the two beams on the bottom of the damper, in the middle, near the two lower edge corners (white dots in Fig. 4b, to be seen on the damper bottom reflected by the prism). The LDV equipment and reflective setup lies on a cast iron bench which isolates the instrumentation. In order to ensure that the noise on the LDV equipment is negligible, tests were performed with accelerometers placed along the three axis on the base of the LDV setup. Fig. 5a shows the FRFs measured by means of LDV compared to the noise coming from the cast iron benches. The signal-to-noise ratio is in this case of the order of magnitude of 10^3. This control was also performed close to the dummy blades (Fig. 5b) to verify that the fixture displacements near the prism were negligible with respect to the measured displacements on the damper.

The LDV setup measures the amount of rolling and vertical translation of the damper on the frontal plane for the two examined modal shape, IP and OoP. LDV measurements are also extended to the blade platforms to measure relative vertical motions between damper and platforms. The two accelerometers placed on the blade platforms at the same height of the contact surfaces (Fig. 3a) overcome the difficulty to measure damper horizontal motion, since the local horizontal motion of the blades can be used to imply damper motion along the same direction. In order to get the whole set of measurements, the LDVs must be redirected through micro-controllers on the mirror of Fig. 4b. Since the measurements are not simultaneous, phase registration of the measurements is crucial. The force transducer signal is used as phase reference. In order to compare the

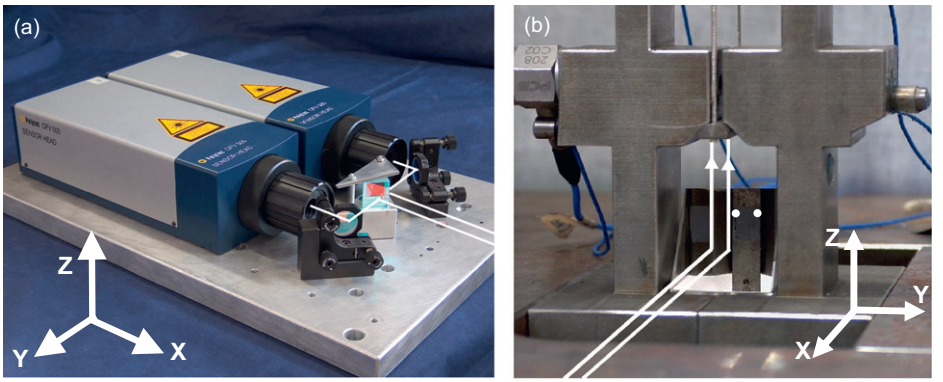

Fig. 4. (a) LDV vibrometers Polytech OFV-505 and (b) prism near the dummy blades base.

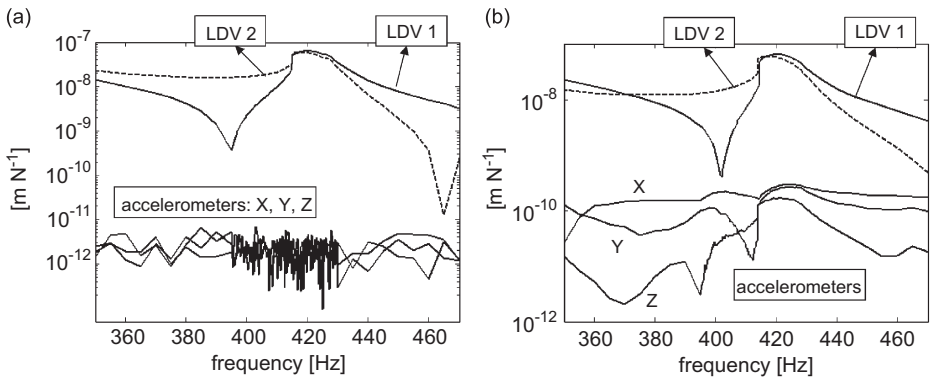

Fig. 5. (a) Damper response compared to the cast iron bench response along *X*, *Y*, *Z* direction and (b) damper response compared to the test rig base response along *X*, *Y*, *Z* direction.

measurements with the numerical simulation outputs in terms of displacement, each measured velocity signal is converted into a Fourier series and each order is integrated to obtain the correspondent displacement value. The resulting harmonics in terms of displacement are summed up in order to obtain the total motion. The process is applied to all the tests here presented.

4. Cylindrical damper in stick condition

4.1. Dynamic response of the dummy blades in stick condition

Step sine tests are performed with a loading ratio $CF/F_e = 350$ which, according to analysis, corresponds at full stick state of the damper against the blade platforms. The test is performed within a range of frequencies wide enough to study the change of the dynamic behaviour of the two dummy blades interacting with the cylindrical damper for IP and OoP modes.

Fig. 6 shows two FRFs measured with the accelerometer placed at the tip of the directly excited blade. One FRF refers to the structure without the damper (free-structure) and the other is the FRF with the fully stuck damper (stick-structure). The free-OoP peak is well evident at 293 Hz, very close to the free-IP peak at 296 Hz (not visible in Fig. 6 because overlapped by the free-OoP mode). The cylindrical damper couples the two blades in fully stuck condition generating the same tip amplitude of vibration for both, during IP and OoP vibration. However, the stiffening effect produced by the damper for the two modes is different: this is visible by looking at the relevant difference in frequency. The stick-OoP mode is stiffened up to 418 Hz (+40%), while the stick-IP slightly decreases from 296 to 294 Hz. The cylindrical damper does not produce a stiffening effect in IP mode, the softening effect is due to the addition of the mass of the damper to the dummy blades. The different change of the resonant frequencies is caused by a different kinematic behaviour of the cylindrical underplatform damper which will be discussed in the next section.

4.2. Kinematics of the cylindrical damper in stick condition

Tests in time domain are performed during IP and OoP vibration. A sinusoidal excitation force with $F_e = 1$ N excites the structure at the two resonant frequencies. During IP vibration, the cylindrical damper shows a rolling motion which avoids sliding displacement at the contact surfaces. This is demonstrated through LDV measurements. LDV beams measure vertical velocities at points 1, 4 on the platforms (Fig. 7), and at points 2, 3 on the damper. Points 2′ and 3′ are the geometrical contact point between damper and

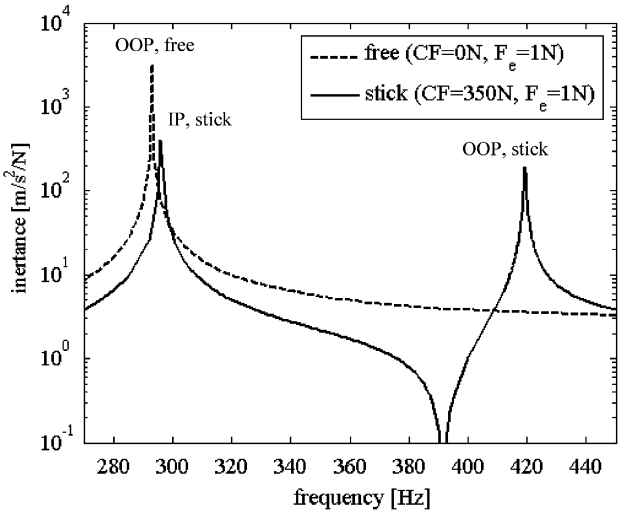

Fig. 6. Free and stick experimental response of the directly excited blade coupled with the cylindrical damper.

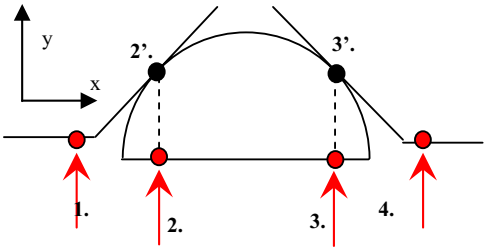

Fig. 7. Positions where the LDV measures the vertical displacements.

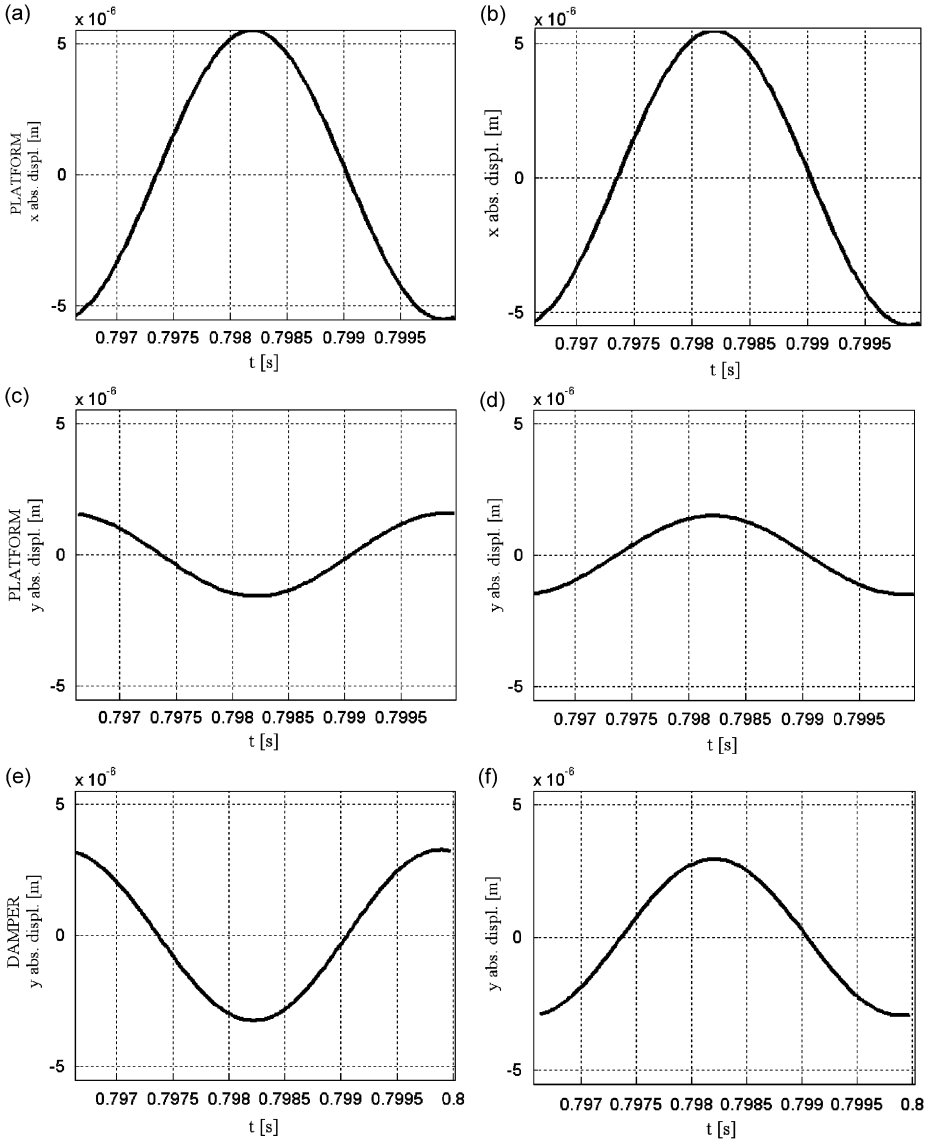

Fig. 8. Cylindrical damper, IP mode: horizontal platform displacements ((a) left and (b) right), vertical platform displacements ((c), point 1 and (d), point 4) and damper ((e), point 2 and (f), point 3) vertical motions.

platforms, they are aligned along vertical directions with points 2 and 3. Figs. 8a and b shows the blade platforms vibrating along the horizontal direction in phase with the same amplitude, while damper vertical displacements are two harmonics at 180°, like platform vertical displacements. Rotation of the cylindrical

damper is consistent with displacements of the platforms and with rolling at the contact points. The blade platforms rotate clockwise when the damper rotates counter-clockwise. It is easy to demonstrate, from values recorded in Fig. 8, that during IP vibration the cylindrical damper experiences a rolling motion around the contact lines damper/platform. This is obtained through a graphical construction of instantaneous velocities or by a simple FE model where the mating contact is substituted by a hinge-link between two nodes (Fig. 9). In a first approximation and due to the small displacements of the damper, the FE congruence of the mating node displacements is equivalent to the real rolling contact motion. Furthermore, a horizontal motion of the cylindrical damper driven by the IP horizontal vibration of the blades can be evaluated from the FE simulation. In the measurements under analysis it can be inferred from the platform accelerometers (Figs. 8a and b) that the cylindrical damper is subjected to a horizontal translation whose amplitude is bigger than the vertical LDV measurements near the damper edges (Figs. 8e and f).

The same condition is simulated with the full numerical code which includes the elastic and sliding contact parameters (Fig. 10). It is found that in the IP case no sliding occurs, and, as it should be expected, the values assigned to the contact parameters (tangential and normal contact stiffness, friction coefficient) do not influence the response.

On the contrary the stick-OoP is strongly dependent on contact stiffness values, and therefore it is a useful test to quantify the contact stiffness at the contact interface. In this case, in fact, a hinge constraint on the FE

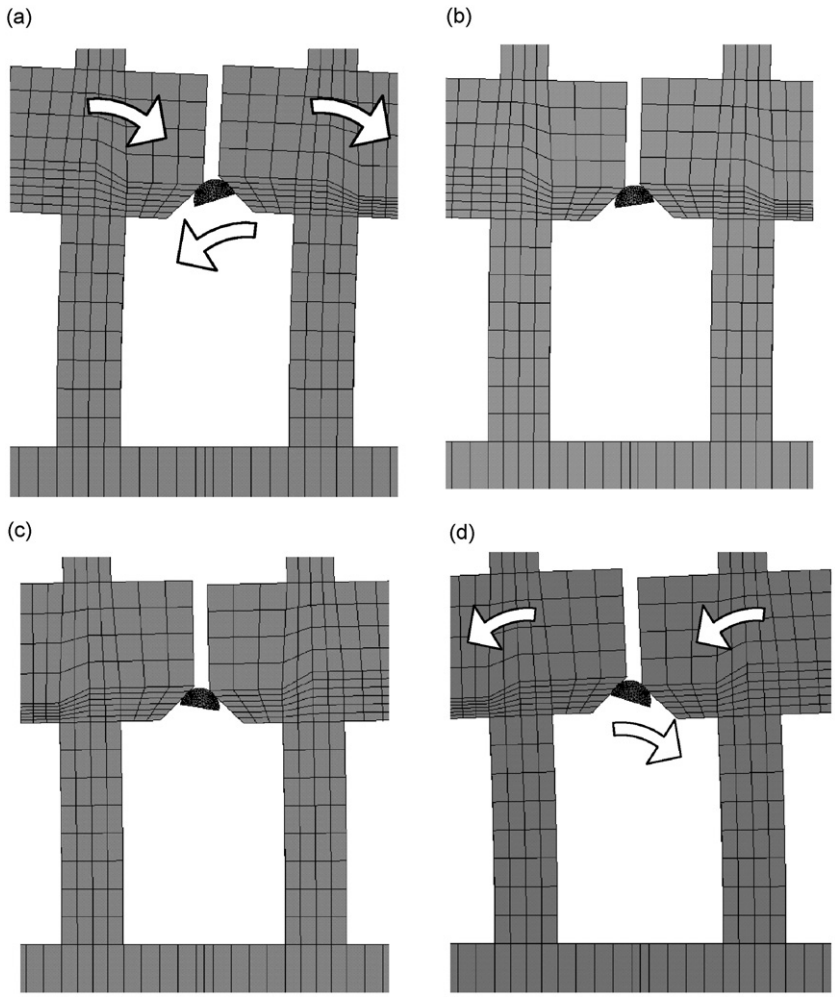

Fig. 9. FE simulation of a rocking kinematics of the cylindrical damper, frames (a) to (d) cover a half period: (a) $t = 0$, (b) $t = T/6$, (c) $t = T/3$, and (d) $t = T/2$.

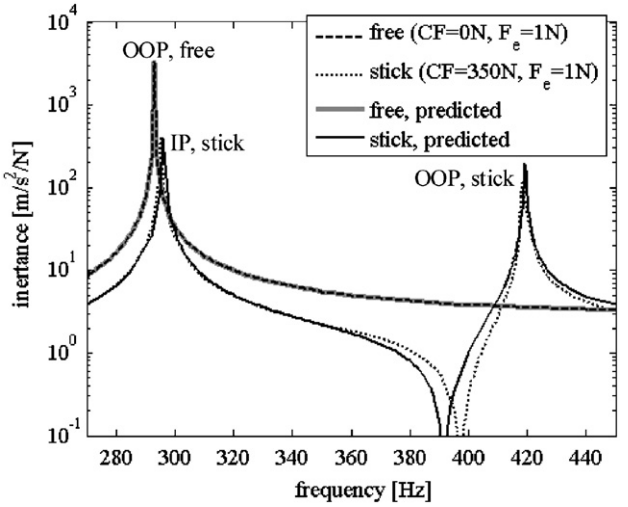

Fig. 10. Numerical-experimental comparison for the free and stick response with the cylindrical damper.

Table 1
Contact stiffness values as a function of the number of contact elements per side.

Number of contact elements per side	Contact stiffness k ($\mathrm{N\,m^{-1}}$) for tuning
6	2.5×107 (used)
4	5×107
2	1×108

model overestimates the stiffening effect. The use of contact elements with assigned tangential k_t and normal k_n contact stiffness is necessary; k_t and k_n are tuned with curve fitting, under the assumption $k_t = k_n = k$. The value k is a function of the number of contact elements for contact area (Table 1), the choice is a compromise between the increasing computational time required by the increasing number of contact elements and the need for a discretization of the contact area refined enough that the point-load approach does not significantly diverge from reality, i.e., a distributed contact load.

The combination of LDV and accelerometers measurements in time domain (Fig. 11) demonstrate that the damper trajectory results in a vertical translation (Figs. 11e and f) during OoP blades vibration (Figs. 11a and b). A very minor damper rotation (visible looking at points 2 and 3 whose amplitude of vibrations are shown in Figs. 11c and d and horizontal motion are due to a not identical symmetry of system vibration and contact elastic conditions.

5. Wedge damper in stick condition

5.1. Dynamic response of the dummy blades in stick condition

Fig. 12 shows two measured FRFs of the directly excited blade at the same loading condition of the cylindrical damper, using the same transducer. The stick-FRF using the wedge damper is similar to the stick-FRF of the cylindrical damper, in detail:

- The blade amplitude for both peak responses is about 15% lower than those using the cylindrical damper.
- The OoP mode shifts towards higher frequencies with a 46% increase against 43% using the cylindrical damper.

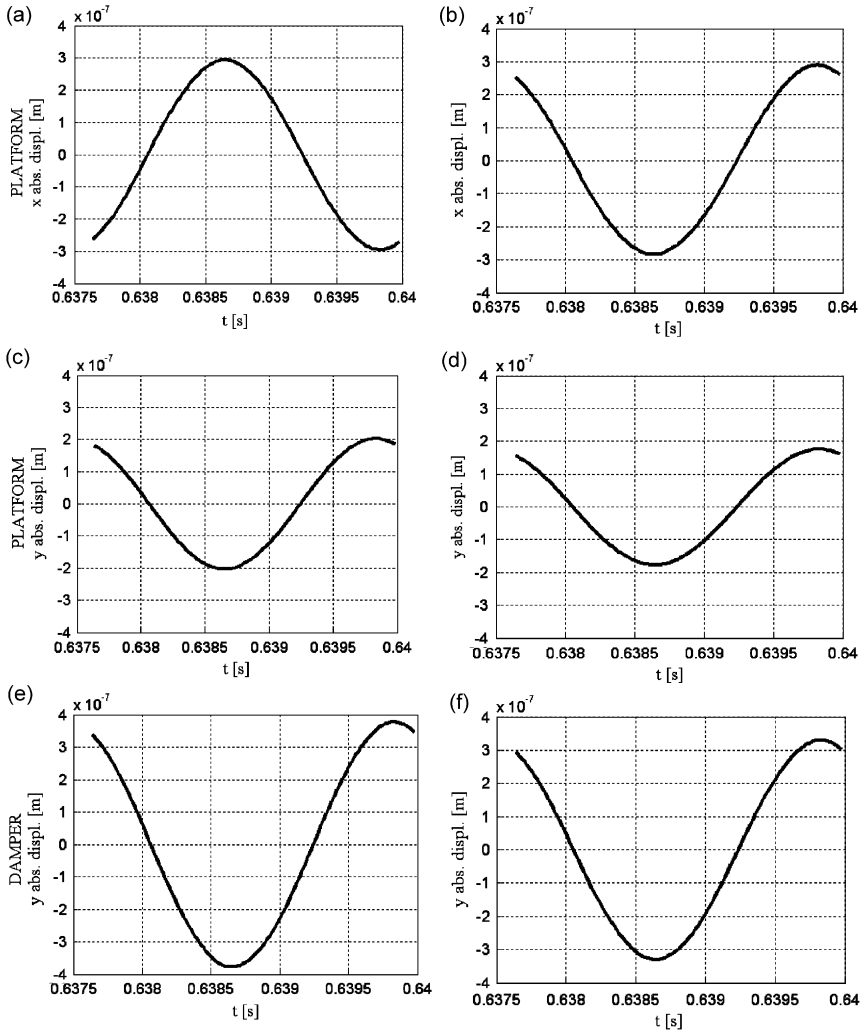

Fig. 11. Cylindrical damper, OoP mode: horizontal platform displacements ((a) left and (b) right), vertical platform displacements ((c), point 1 and (d), point 4) and damper ((e), point 2 and (f), point 3) vertical motions.

Instead, the IP modal shape depends on the CF/F_e ratio which in stick response increases the IP resonant frequency of 14% with respect to the free-IP response. Flat surface contacts in this case stiffen the IP mode and influence the damper kinematics.

5.2. Kinematics of the wedge damper, stick condition

The kinematics of the wedge damper in OoP vibration is characterized again by a translation motion: in particular Figs. 13c and d show that the vertical amplitude of vibration is smaller than the amplitude of the cylindrical damper. On the contrary IP vibration is characterized by a rolling motion between the two platforms (Fig. 14). The damper rotation is smaller than the cylindrical rocking motion and the stiffening effect of the IP modal shape visible in Fig. 12 proves that is not possible to simulate the constraint with a 'hinge' model. Since also in this case the blade platforms rotate clockwise when the damper rotates counter-clockwise, either local lift-off of the contact regions occurs, or the distributed normal compliance of the flat punch contacts of the damper allows the pressure distribution to vary locally within one oscillation. In order to simulate this type of contact, the position and the number of the contact elements to place must be chosen. A nonlinear static FEM analysis is helpful to determine the real contact area. Ordinary contact elements

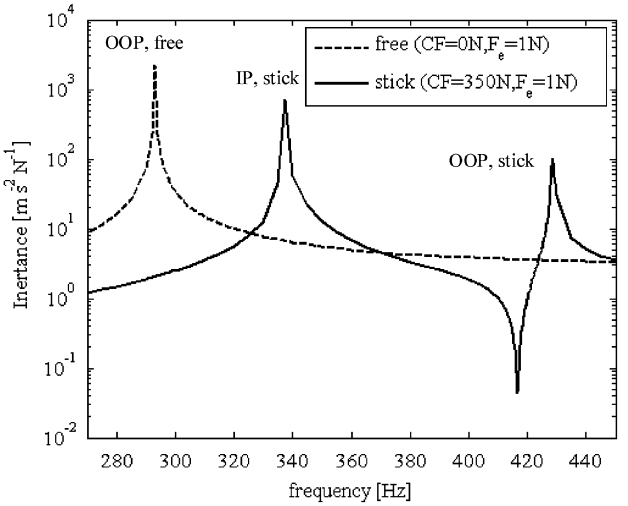

Fig. 12. Free and stick experimental response of the directly excited blade coupled with the wedge damper.

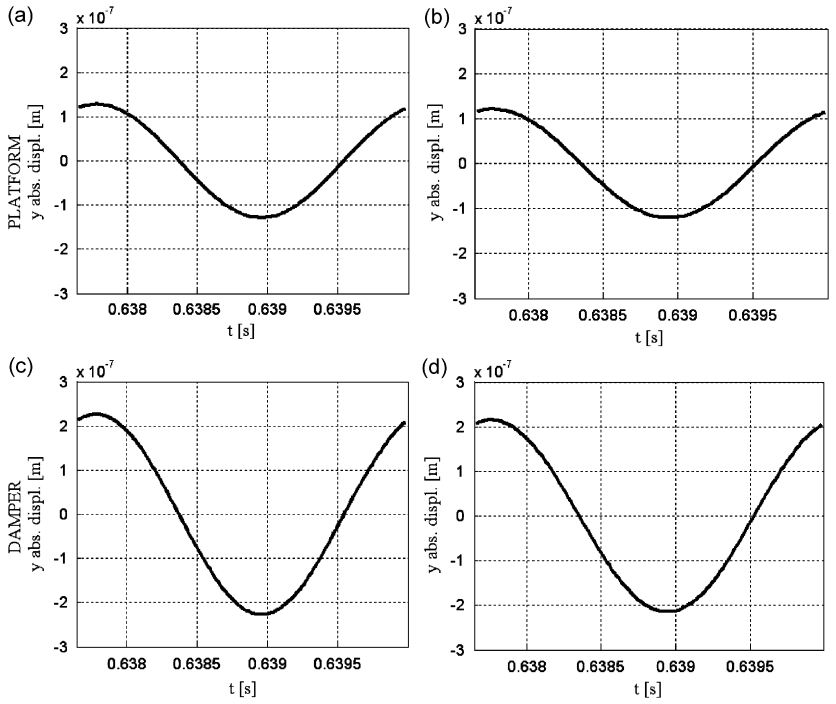

Fig. 13. Wedge damper, OoP mode: platforms ((a), point 1 and (b), point 4) and damper ((c), point 2 and (d), point 3) vertical motions.

provided by commercial codes are used along the nominal contact area and a pulling load is applied to the damper as in the test rig. The result is not sensitive to the values of the contact parameters to input in the commercial code in its contact element. The simulation shows that eight master nodes per side placed in the central part of the contact area are a suitable choice to couple the wedge damper with the dummy blades through the contact elements modelled for friction damping in the nonlinear numerical code (dots in Fig. 2).

The same curve fitting procedure used for the cylindrical damper is here used to update the value of contact stiffness of the wedge damper case. The numerical FRFs match with good accuracy the measured FRFs for both stick-IP and stick-OoP mode if the same values used for the cylindrical damper are adopted (Fig. 15).

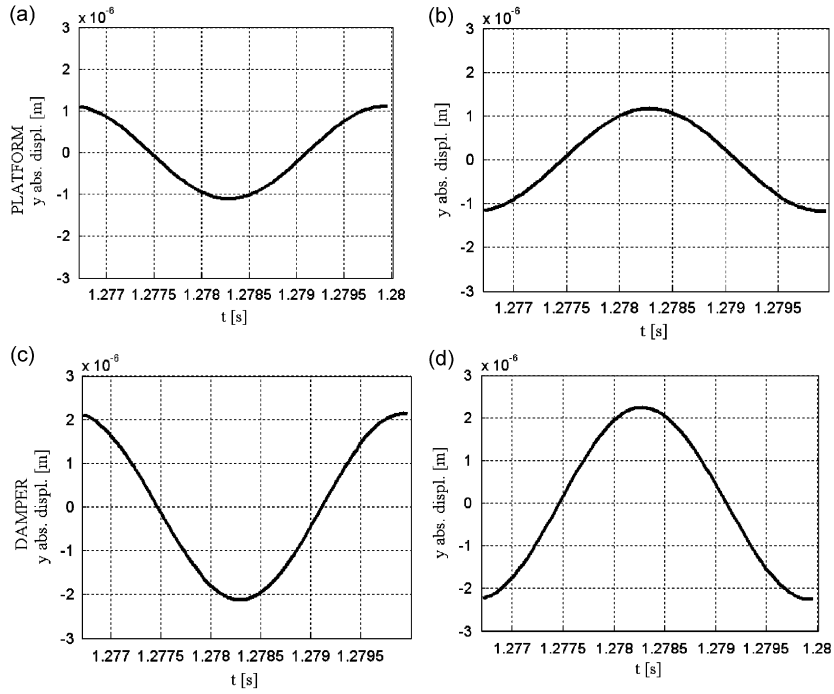

Fig. 14. Wedge damper, IP mode: platforms ((a), point 1 and (b), point 4) and damper ((c), point 2 and (d), point 3) vertical motions.

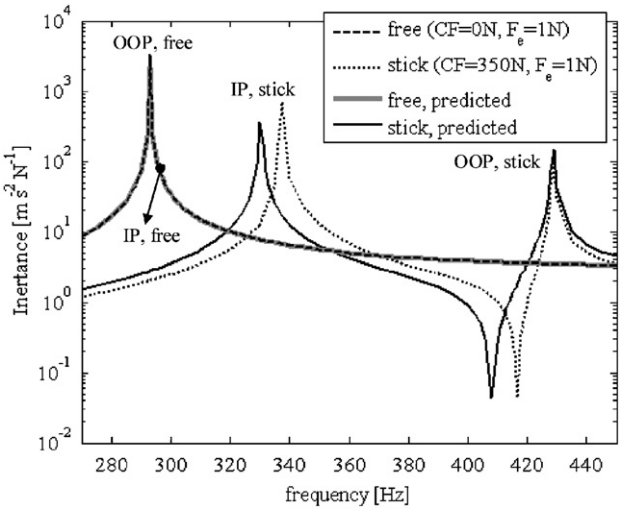

Fig. 15. Numerical-experimental comparison for the free and stick response with the wedge damper.

6. Cylindrical damper in slip condition

The same tests in frequency domain are performed for lower CF/F_e values in order to have slip at the contact surfaces. For this reason CF/F_e ratio is gradually decreased from 350 to 4. Fig. 16a shows the trend the FRF follows for IP and OoP modal shapes.

IP vibration appears almost insensitive to CF/F_e ratio, and damping in IP mode is so small that frequency response tests at resonance (Fig. 16b) must be limited to $F_e < 4$ N, due to the acquisition system characteristics. During these tests, LDV measurements of platforms and damper are taken; all of them showed pure rolling motion of the cylindrical damper. In order to assess damper behaviour at the highest possible excitation, LDV

measurements in time domain have been taken up to $F_e = 9$ N, where FRF step sine tests are not possible due to the failure of the feedback control.

As Fig. 17 shows, measured displacements do well compare with rolling motion as predicted by FEM stick conditions: in fact the LDV measurements on the bottom of the cylindrical damper together with the output signals of the four accelerometers show the same deflection shape measured in stick condition, scaled of a factor slightly smaller than 11 at the tip of the blades.

The cylindrical damper is effective for the OoP mode (Fig. 16a), and its effect is clearly visible already for small F_e values (Fig. 16c).

A nonlinear calculation was performed with the numerical code in order to simulate the gross-slip in OoP vibration. In this case the friction coefficient is the contact parameter which determines the amount of damping. This parameter is not known a priori and it has to be tuned against experimental evidence. In the calculation the value 0.7 has been adopted through curve fitting of the damped OoP peak measured at the tip of the two dummy blades for $CF/F_e = 4$. Comparison with experimental data of the cylindrical damper trajectory for the OoP mode is shown in Fig. 18. Each frame is divided into three figures. The figure in the centre shows the calculated simulation of the damper trajectory. The dashed line represent the damper in static condition. Circle markers on the cylindrical surface show the position of the contact elements. LDV beams are the vertical lines hitting the damper base. The x-axis and y-axis coordinates are the geometrical coordinates of the damper FE models. A scale factor of 200 is applied to both numerical and experimental data to make them visible. The left and right figures show respectively the directly and indirectly excited blade platforms. The same graphical notation used for the underplatform damper holds. Furthermore, the arrows at the contact points of the damper in the central figures are the forces the damper exerts on the platforms. They are the

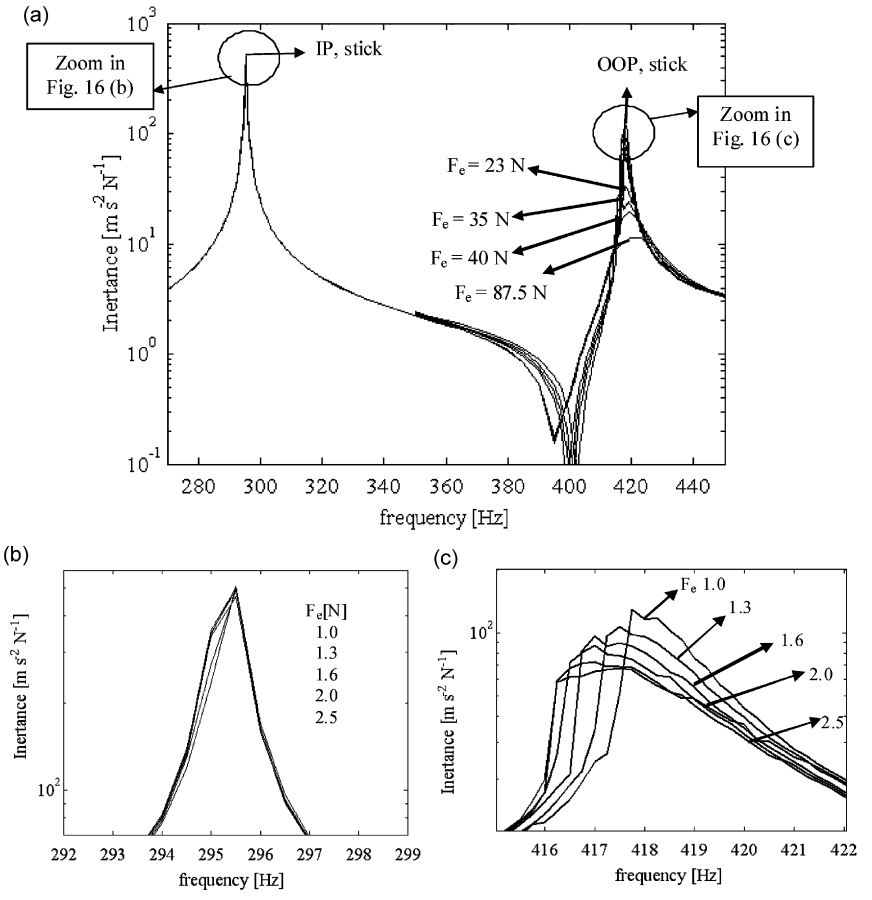

Fig. 16. (a) Cylindrical damper, nonlinear experimental responses, (b) IP zoomed responses, and (c) OoP zoomed responses.

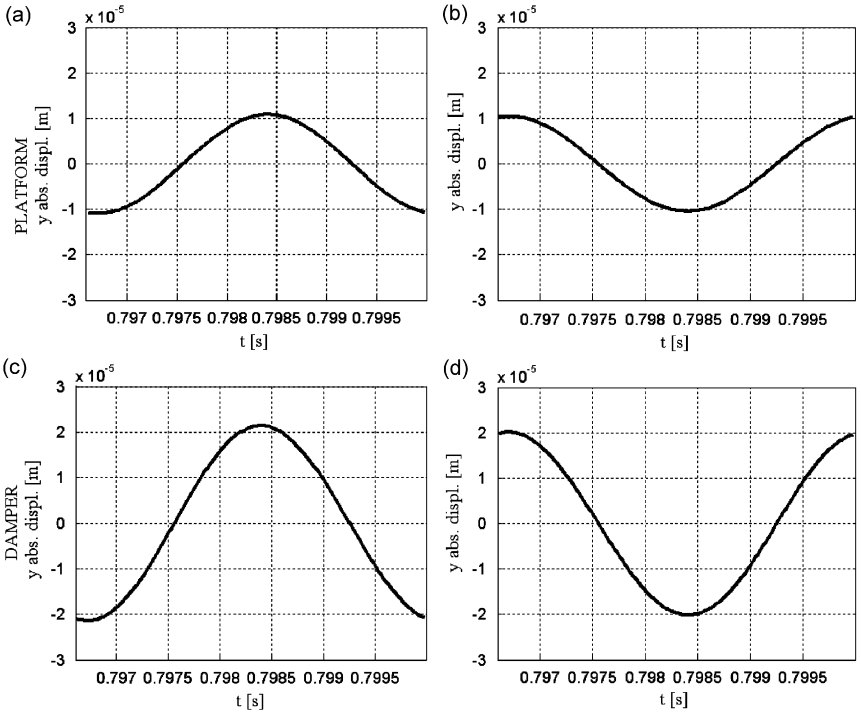

Fig. 17. Cylindrical damper, $CF/F_e = 39$, IP mode: platforms ((a), point 1 and (b), point 4) and damper ((c), point 2 and (d), point 3) vertical motions.

result of the composition of the tangential and normal contact force vectors. The state for each contact point (stick, slip, lift-off) is also reported. The predominant kinematics is a vertical translational motion with a small amount of rotation. A phase shift between the numerical simulation and the LDV output signals is shown, but the comparison is good over all. A single experimental-numerical comparison of a measured point shows better the correspondence of the two results and it permits to see the effectiveness of the HBM approximation in the calculation procedure. Fig. 19a shows a velocity signal of the left edge of the cylindrical damper during gross slip vibration within the fundamental period of the excitation force F_e. The output signal includes nonlinear super-harmonics components generated by sliding. Fig. 19b shows the comparison between the measured motion in terms of displacement as described in Section 3.1 and the simulated result. It can be seen that the whole motion is characterized by a small nonlinearity and that can be well approximated by HBM linearization.

7. Effect of the wedge damper in slip condition

The same tests performed on the cylindrical damper were repeated also for the wedge damper. Fig. 20 shows the damped FRFs for CF/F_e ratio decreasing to the value of 4. The wedge damper proves to be as effective in reducing the OoP peak amplitude as the cylindrical damper.

Also in this case the attention is mainly focused on IP response. Similarly to the cylindrical damper case where the damping amount is low, the maximum level of external excitation in IP measurements is bounded by the force drop off phenomenon. In this cases, a maximum level of $F_e = 13$ N has been used, almost three times the maximum value acceptable for the cylindrical damper, concluding that the wedge damper is more effective in damping IP vibration than the cylindrical dampers. More accurate comparisons are not possible due to the lack of reliable measurements, since during all the measurements performed around the IP resonance the maximum iteration number introduced in Section 3 is reached.

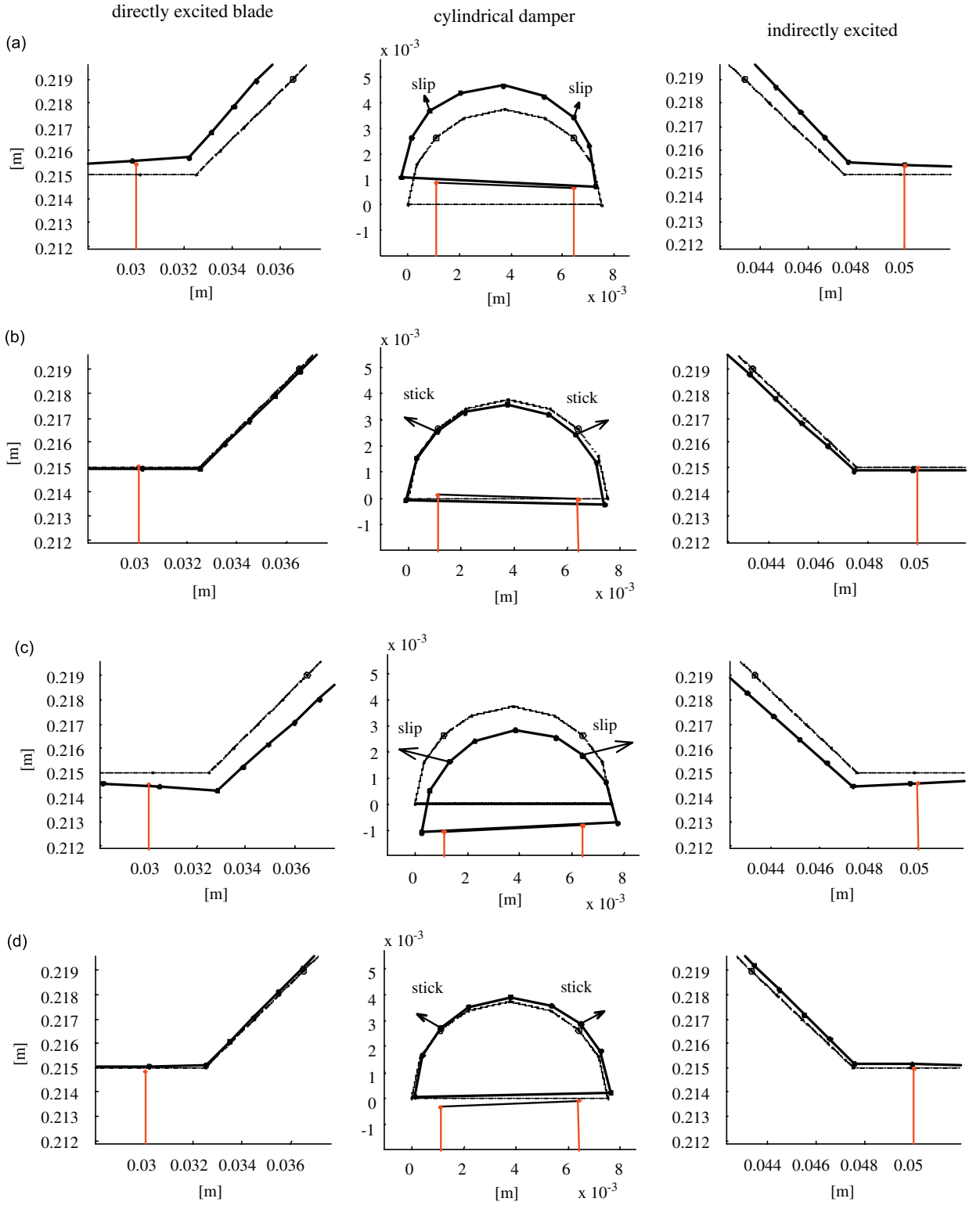

Fig. 18. Cylindrical damper, one oscillation during OoP vibration: numerical-experimental comparison of the nonlinear response for $CF/F_e = 4$ (displacement are multiplied by a factor of 200): (a) $t = 0$, (b) $t = T/4$, (c) $t = T/2$, (d) $t = T(3/4)$.

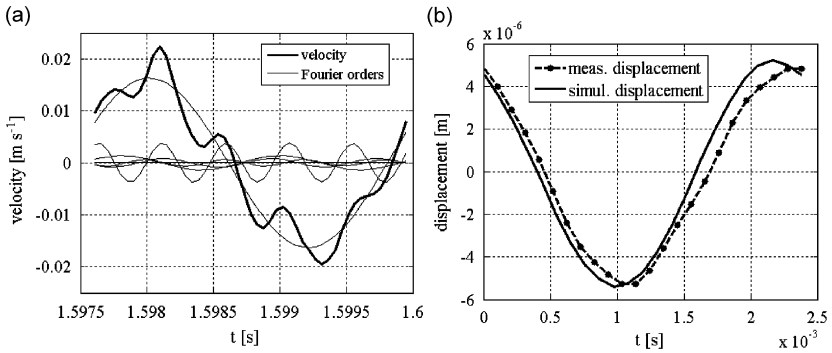

Fig. 19. (a) Velocity measurement during gross-slip on the damper left edge. The nonlinear signal is split in its Fourier components and (b) real nonlinear displacement compared to the simulation.

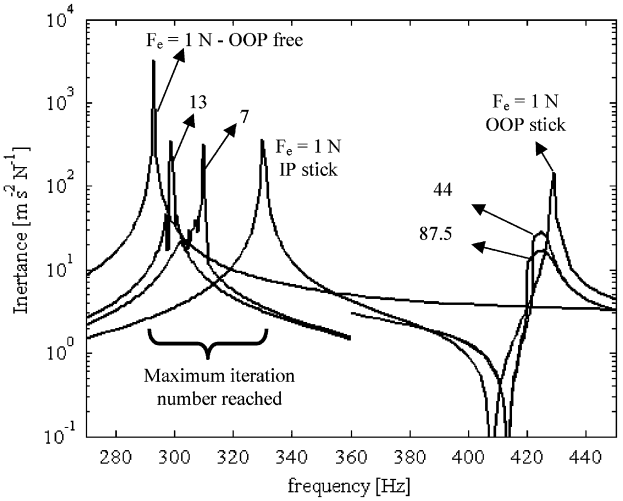

Fig. 20. Wedge damper, nonlinear experimental responses.

LDV measurement of Fig. 21 shows that points 1 and 2 move in phase as well as points 3 and 4, like in the case of the cylindrical damper where points 1–2 move upward and points 3–4 move downward alternatively within one oscillation.

It is here demonstrated that this evidence is in contrast with the kinematics resulting from a contact model which predicts the full contact between the two damper/platform flat surfaces. In this case in fact the following hypothesis must be assumed:

- When two dummy-blades vibrate in an IP bending mode the deflection displacements for the two blades is the same, therefore the angle between the two platforms remains constant during motion.
- This angle is exactly equal to the angle between the two contact surfaces of the wedge damper, under loading condition.

Only in this case the wedge damper has the possibility to slip at the contact keeping the flat surfaces in full contact with the blade platforms during the whole IP vibration.

Fig. 22 shows a FEM simulation using a linear constraint equation in order to represent the kinematics corresponding to this classic "slider" model; it can be clearly seen that this contact model produces a downward motion of point 1 while point 2 has an upward motion; reverse situation for points 3 and 4.

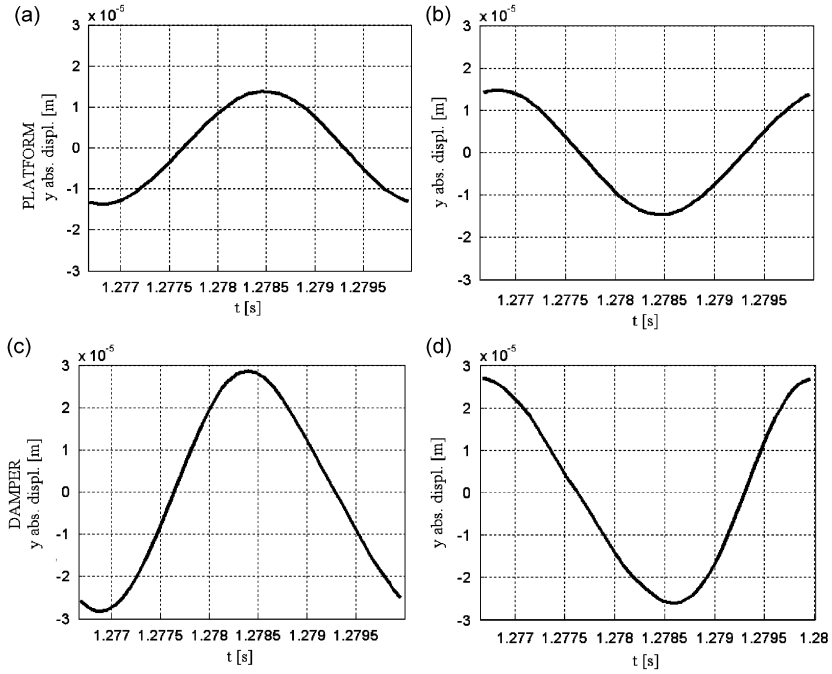

Fig. 21. Wedge damper, IP Mode: platforms ((a) point 1 and (b) point 4) and damper ((c) point 2 and (d) point 3) vertical motions.

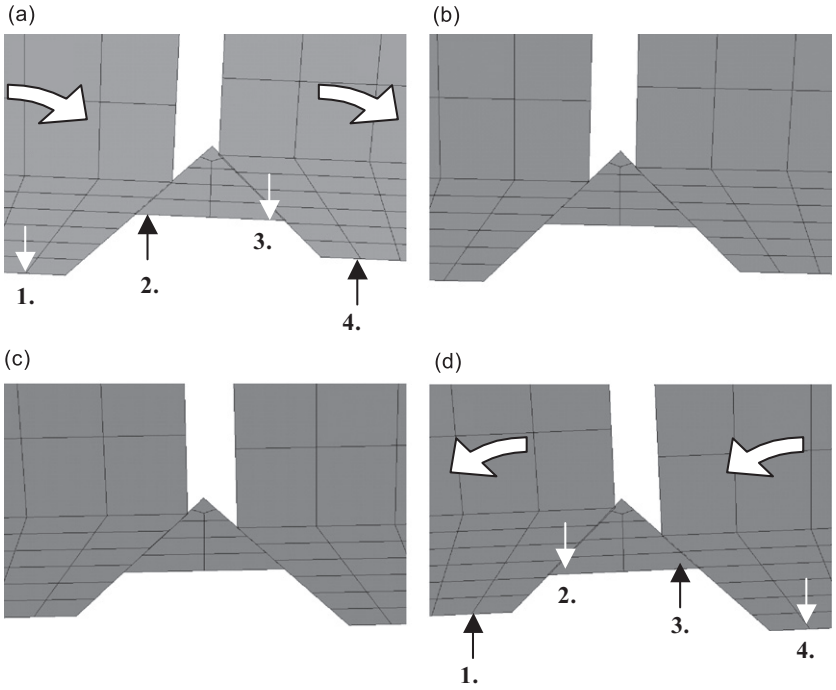

Fig. 22. Wedge damper, FE simulation of a 'slider' kinematics model, frames (a) to (d) cover a half period: (a) $t = 0$, (b) $t = T/6$, (c) $t = T/3$, (d) $t = T/2$.

The slider "model" is in conflict with experimental findings. In fact, LDV measurement of Fig. 21 shows that points 1 and 2 move in phase as well as points 3 and 4. The most evident difference stands in the sign of the damper rotation with respect to the platforms: the "slider" model predicts the same sign of rotation both for

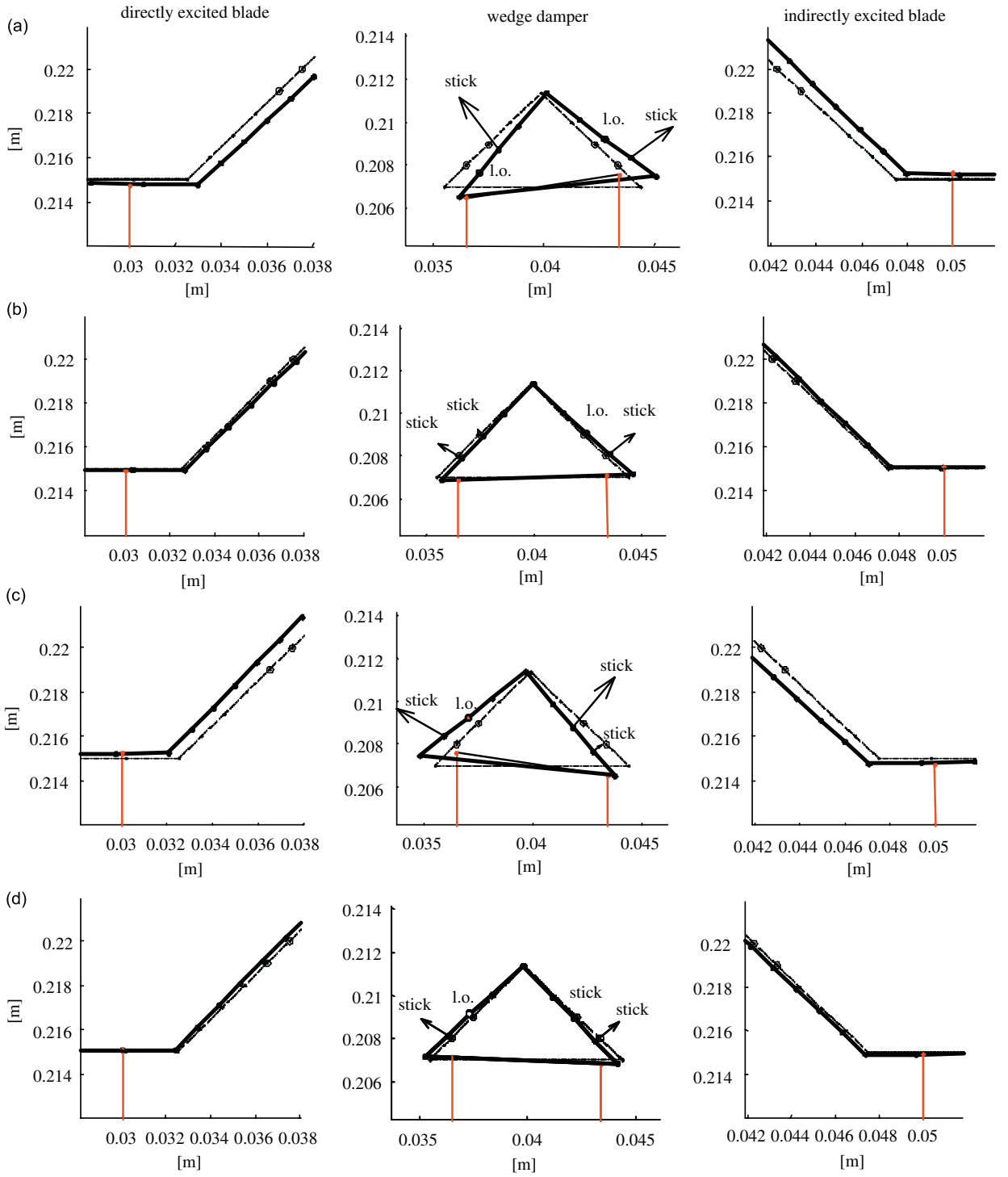

Fig. 23. Wedge damper, one oscillation during IP vibration: numerical-experimental comparison of the nonlinear response for $CF/F_e = 12$ (displacement are multiplied by a factor of 20): (a) $t = 0$, (b) $t = T/4$, (c) $t = T/2$, (d) $t = T(3/4)$.

damper and platforms, while the experimental measurements show that the damper rotation has an opposite sign to the blade rotation. This test in time domain is extended up to $CF/F_e = 12$, i.e. $F_e = 29$ N. Since it is not possible to measure an FRF which indicates exactly the IP resonant frequency, several tests in time domain

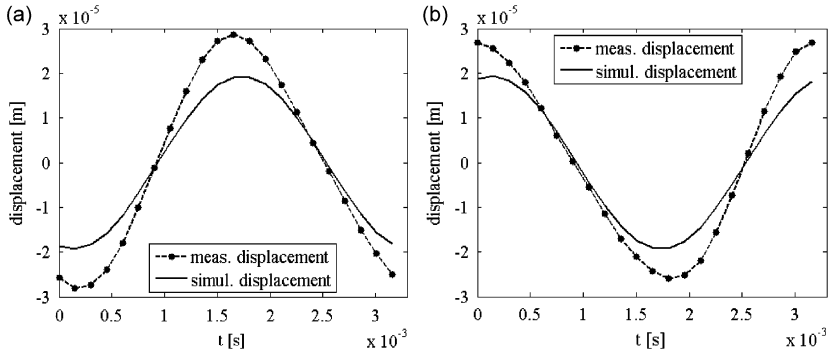

Fig. 24. Numerical-experimental comparison of: (a) left and (b) right edge of the wedge damper during IP vibration.

were performed with different excitation frequencies and a supposed resonance frequency of 302 Hz was chosen corresponding to the highest response amplitude.

A nonlinear simulation was performed for the IP mode at $CF/F_e = 12$. The damper trajectory corresponding to one oscillation was then plotted for the peak response obtained by the calculation. The resulting kinematics reveals a rolling trajectory with partial lift-off of the contact surfaces within one period of oscillation (Fig. 23). Two pair of nodes per section has been chosen and placed on the contact surfaces as suggested by the nonlinear static FEM analysis (Fig. 2). The FE result is consistent with the wear produced on the underplatform damper.

The partial lift-off of the contact surface is indicated by the label 'l.o.' over a contact point. In this case the contact forces go to zero. It is possible to note that damper nodes still in contact with the platforms are always in stick condition. Nonlinear behaviour of the wedge damper is due to the lift-off and stick condition alternating state, not by tangential slipping. The simulation predicts the absence of damping in agreement with experimental findings where the deflection shape results almost in a mono-harmonic oscillation as shown in Fig. 24a and b. The simulation showing partial lift-off of the wedge damper in conjunction with its rocking motion kinematics is also in agreement with the simulation performed in Ref. [23]. Simulation for OoP mode shows results similar to those already discussed for the OoP cylindrical damper (predominant vertical translation leading to a gross-slip contact state); they will not be discussed here.

8. Conclusion

The link between the kinematic behaviour of two representative types of underplatform dampers, experimentally detected by means of a novel approach based on LDV measurements, and their damping capability has been explored. The study of a cylindrical and wedge underplatform damper was focused on two particular first bending modes of a two dummy blades system: "in phase-IP" and 180° "out of phase-OoP" modal shapes.

The kinematic behaviour of cylindrical and wedge dampers, when blades vibration is OoP, is substantially identical: LDV measurements show that the trajectory of the two dampers is a predominant translation. As expected, experiment shows that also damping is strictly equivalent: for a value of $CF/F_e = 4$, which ensures gross-slip for both dampers, the two dampers produce an amplitude reduction, compared both to free and to stick conditions, of more than 90% in both cases.

During IP vibration the cylindrical damper experiences a pure rolling motion at the contact points, which makes it almost ineffective for damping and produces a linear dynamic behaviour for all CF/F_e ratios. LDV measurements show a damper rotation in agreement with rigid body kinematics, i.e., opposite to the rotation of platforms.

In the case of the wedge damper, experiments detected a kinematic behaviour in contrast with the rigid body slider model: in fact rotation is found to be opposite to the rotation of platforms, while the slider model implies an equal angle of rotation both in sign and magnitude. The rocking motion occurs in stick and in expected slip cases, and is permitted by the presence of elastic compliance in the direction normal to the

contact surfaces. The behaviour is not linear, and damping, although present, is much lower than according to the slider model. The rocking of the wedge damper with respect to platform rotations measured by the LDV suggests partial lift-off of the contact surfaces occur.

Nonlinear numerical simulations support experimental evidence. The FE models were tuned to the linear response of the test rig. Nonlinear contact elements were placed according to nonlinear static analysis with FEM commercial software. Nonlinear macro-slip contact model was adopted since the comparison with experimental data was carried out for $CF/F_e = 4$, at which gross-slip is supposed. The numerical-experimental comparison for the OoP mode are good, both for the dynamic behaviour of the dummy blades and for the kinematics of the two dampers. The simulated responses predict a predominant vertical translation of the two underplatform dampers that is consistent with LDV and accelerometers measurements. The comparison shows that HBM linearization is a valuable tool to represent underplatform dampers working in gross-slip regime.

IP simulation reveals a rocking motion kinematics of the wedge damper compatible with LDV measurements evidence. An important conclusion is that the study here presented rules out all pure rigid body models, like slider models, as well as models with no rotational degree of freedom, like mass-point models. Instead, at least two nodes along the height of the contact surface are required to represent the tilting motion of the damper with respect to the blade platforms.

Acknowledgement

The author is grateful to Prof. Muzio Gola for having shared his leading idea of damper kinematics measurement and for all the precious suggestions given to discuss it in this paper.

References

[1] B.D. Yang, C.H. Menq, Characterization of contact kinematics and application to the design of wedge dampers in turbomachinery blading: part 2-prediction of forced response and experimental verification, *ASME Journal of Engineering for Gas Turbine and Power* 120 (1998) 418–423.

[2] L. Panning, W. Sextro, K. Popp, Optimization of interblade friction damper design, *Proceedings of ASME Gas Turbine and Aeroengine Congress and Exhibition*, Munich, 2000-GT-541.

[3] E.P. Petrov, D.J. Ewins, Analytical formulation of friction interface elements of nonlinear multi-harmonic vibrations of bladed discs, *Proceedings of ASME Turbo Expo*, Amsterdam, 2002-30325.

[4] G. Csaba, Modelling of a microslip friction damper subjected to translation and rotation, *ASME Gas Turbine & Aeroengine Congress and Exhibition*, Indianapolis, 1999-GT-149.

[5] K.Y. Sanliturk, D.J. Ewins, A.B. Stanbridge, Underplatform dampers for turbine blades: theoretical modelling, analysis and comparison with experimental data, *ASME Gas Turbine & Aeroengine Congress and Exhibition Indianapolis*, 1999-GT-335.

[6] M.H. Jareland, Experimental investigation of a platform damper with curved contact areas, *Proceedings of ASME Design Engineering Technical Conference*, Pittsburgh, DETC2001/VIB-21391.

[7] M. Jöcker, A. Kessar, T.H. Fransson, G. Kahl, H.J. Rehder, Comparison of models to predict low engine order excitation in a high pressure turbine stage. *Proceedings of the 10th International Symposium on Unsteady Aerodynamimcs, Aeroacoustics and Aeroelasticity in Turbomachines*, Durham, NC, USA, 2003.

[8] J.P. Den Hartog, Forced vibrations with combined coulomb and viscous friction, *Transaction of ASME* (1931) APM-53-9, pp. 107–115.

[9] C.H. Menq, J.H. Griffin, A comparison of transient and steady state finite element analyses of the forced response of a frictionally damped beam, *Journal of Vibration, Acoustics, Stress, and Reliability in Design* 107 (1985) 19–25.

[10] C.H. Menq, P. Chidamparam, J.H. Griffin, Friction damping of two-dimensional motion and its application in vibration control, *Journal of Sound and Vibration* 144 (3) (1991) 427–447.

[11] M. Sanliturk, D.J. Ewins, Modelling two-dimensional friction contact and its application using harmonic balance method, *Journal of Sound and Vibration* 193 (2) (1996) 511–523.

[12] B.D. Yang, M.L. Chu, C.H. Menq, Stick–slip-separation analysis and non-linear stiffness and damping characterization of friction contacts having variable normal load, *Journal of Sound and Vibrations* 210 (4) (1998) 461–481.

[13] B.D. Yang, C.H. Menq, Characterization of 3D contact kinematics and prediction of resonant response of structures having 3D frictional constraint, *Journal of Sound and Vibration* 217 (5) (1998) 909–925.

[14] J. Szwedowicz, M. Kissel, B. Ravindra, R. Kellerer, Estimation of contact stiffness and its role in the design of a friction damper, *Proceedings of ASME Turbo Expo*, New Orleans, 2001-GT-290.

[15] C. Siewert, L. Panning, A. Schmidt-Fellner, A. Kayser, The estimation of the contact stiffness for directly and indirectly coupled turbine blading, *Proceedings of ASME Turbo Expo 2006: Power for Land, Sea and Air*, Barcelona, GT2006-90473.
[16] S. Filippi, E.B. Rodrigues, M.M. Gola, Experimental characterization of contact hysteresis at high temperatures. *ASME Turbo Expo 2006—ASME Conference on Gas Turbines*, Barcelona, GT2006-90757.
[17] K.H. Koh, J.H. Griffin, Dynamic behavior of spherical friction dampers and its implication to damper contact stiffness, *Journal of Engineering for Gas Turbines and Power* 129 (2) (2007) 511–521.
[18] B.D. Yang, C.H. Menq, Characterization of contact kinematics and application to the design of wedge dampers in turbomachinery blading: part 1—stick–slip contact kinematics, *ASME Journal of Engineering for Gas Turbine and Power* 120 (1998) 418–423.
[19] T. Berruti, M.M. Gola, S. Zucca, G.P. De Poli, Underplatform damper performance with turbine blades, *NATO Symposium on Evaluation, Control and Prevention of High Cycle Fatigue in Gas Turbine Engines for Land, Sea and Air Vehicles*, Granada, 2005.
[20] E.P. Petrov, D.J. Ewins, Advanced modelling of underplatform friction dampers for analysis of bladed disc vibration, *Proceedings of ASME Turbo Expo 2006: Power for Land, Sea and Air*, Barcelona, GT2006-90146.
[21] C.M. Firrone, D. Botto, M.M. Gola, Modelling a friction damper: analysis of the experimental data and comparison with numerical results, *Proceedings of ASME ESDA2006*, Torino, ESDA2006-95605.
[22] E.P. Petrov, Explicit finite element models of friction dampers in forced response analysis of bladed discs, *Proceedings of ASME Turbo Expo 2007 Power for Land, Sea and Air*, Montreal, GT2007-27980.
[23] E. Cigeroglu, N. An, C.H. Menq, Wedge damper modeling and forced response prediction of frictionally constrained blades, *Proceedings of ASME Turbo Expo 2007 Power for Land, Sea and Air*, Montreal, GT2007-27963.